

Theoretical Investigations on the Rh(III)-Catalyzed Oxidative C–H Activation/Annulation of Salicylaldehydes with Masked Enynes: Mechanism Insights and Regioselectivity Origins

Xin Xiang, Wei Wei, Zeng-Xia Zhao,* and Hong-Xing Zhang



Cite This: *ACS Omega* 2023, 8, 45109–45114



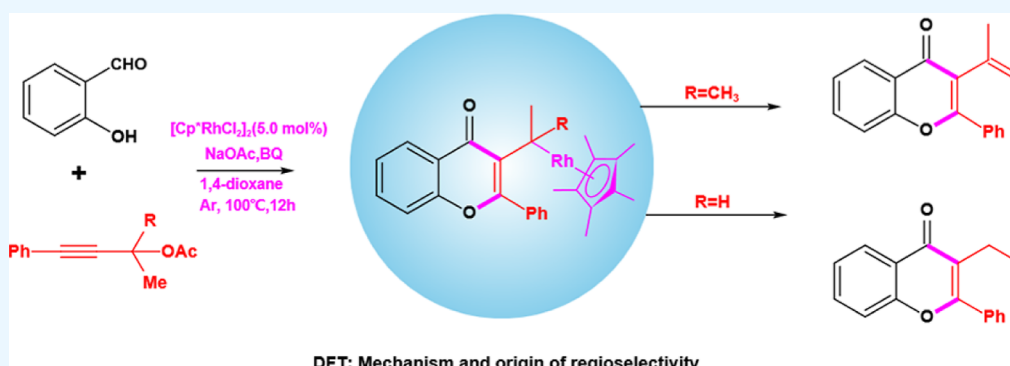
Read Online

ACCESS |

Metrics & More

Article Recommendations

Supporting Information



DFT: Mechanism and origin of regioselectivity

ABSTRACT: The mechanism underlying the rhodium(III)-catalyzed reaction of the C–H alkenylation/annulation reaction of salicylaldehydes with enynes has been thoroughly investigated using DFT calculations. Based on mechanistic studies, our focus primarily lies on the regioselectivity of asymmetric alkynes inserting into the Rh–C bond and the involvement of the auxiliary group OAc[−] in these reactions. Our theoretical study uncovers that, with acetate assistance, a stepwise S_N2′ cyclization, 1,3-Rh migration, β-H elimination, and reductive elimination process occur. Furthermore, we also explore the role of substitution at C_α (CH₃ vs H) in the reaction. As demonstrated in this work, these findings are applicable to other related reactions.

INTRODUCTION

Chromones are a significant class of oxygen-containing heterocycles that are present in natural products and pharmaceuticals, exhibiting noteworthy biological activities such as anti-inflammatory, antimicrobial, antioxidant, and anticarcinogenic properties.^{1,2} The synthesis of chromones can be accomplished through transition-metal-catalyzed sequential C–H activation/annulation of salicylaldehydes with suitable coupling partners.^{3–7} Despite these advanced methods for constructing new skeleton molecules, there is still an urgent need to synthesize new related molecules, such as 3-vinyl chromone,⁸ which is found in many bioactive compounds and has antioxidant, antiproliferative, and PDE10 inhibitory activities,^{9–11} and therefore remains of very important value in organic synthesis.

Recently, Huang and Yao¹² reported the Cp*Rh(III)-catalyzed reaction of salicylaldehydes with propargylic acetates, wherein the enynes are inserted into the in situ generated 3-vinyl chromones (Scheme 1). The corresponding possible reaction mechanisms postulated by Huang, Yao, and co-workers are demonstrated in Scheme 2. At the outset, aldehyde (1a) undergoes C–H activation in the presence of the Rh(III) catalyst to form rhodacycle intermediate I. Subsequently,

propargylic acetate 2a coordinates to the Rh center to give intermediate II, followed by migration into the Rh–C bond of intermediate II to generate intermediate III. With assistance from acetate, the intramolecular S_N2′ cyclization of intermediate III can occur to yield intermediate IV. Further, the 1,3-Rh migration of intermediate IV leads to the formation of intermediate V. When R = H, protonation of benzylic rhodium V results in the production of byproduct 14. β-Hydrogen elimination from intermediate V, followed by reductive elimination, gives product 3a (R = Me) along with Rh(I) species. Oxidation regenerates the active catalyst Rh(III), allowing it to enter the next catalytic cycle.

To gain a deeper understanding of directing group migration in Rh(III)-catalyzed C–H functionalization of salicylaldehydes with propargylic acetates, we conducted DFT calculations to investigate the intricate mechanism of the reaction model. In

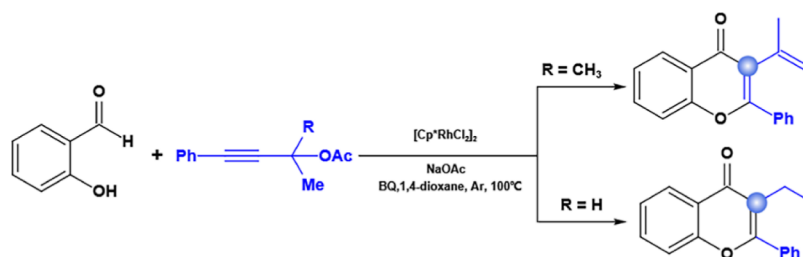
Received: September 24, 2023

Revised: October 31, 2023

Accepted: November 3, 2023

Published: November 17, 2023



Scheme 1. Reaction of Rh-Catalyzed Cascade Reactions of Salicylaldehyde and Propargylic Acetate Reported by Huang and Yao's Group¹²

Scheme 2. Possible Reaction Mechanism Proposed by Huang and Yao's Group

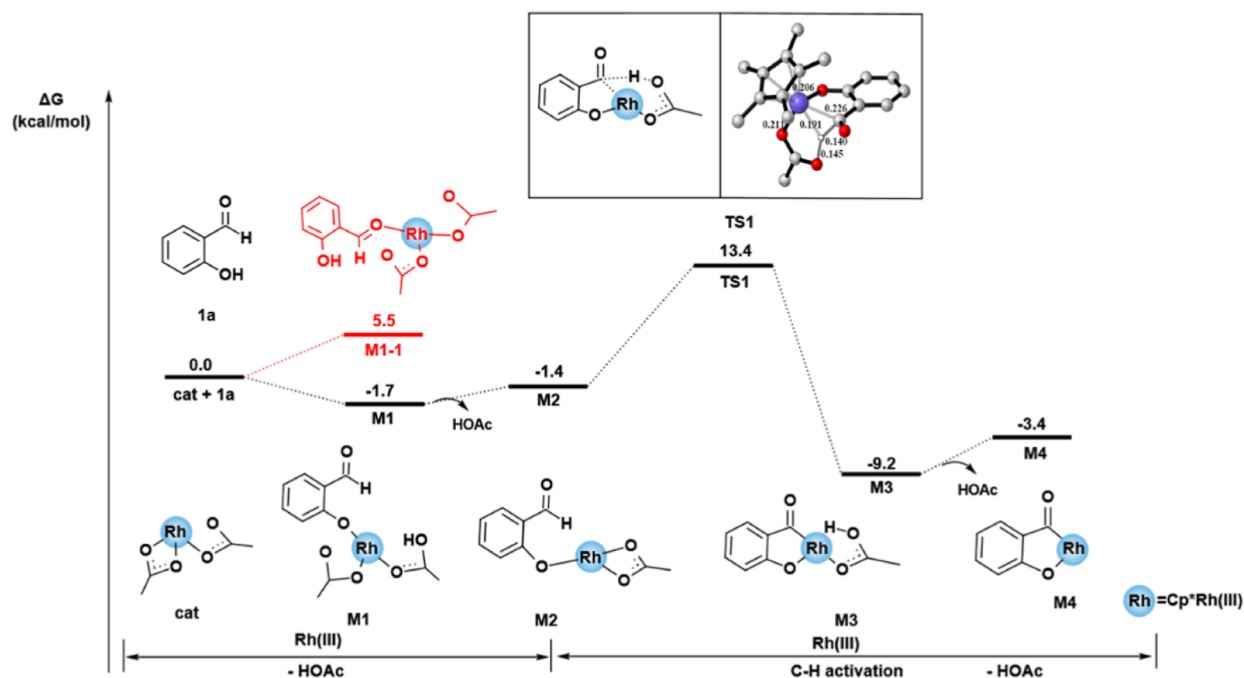
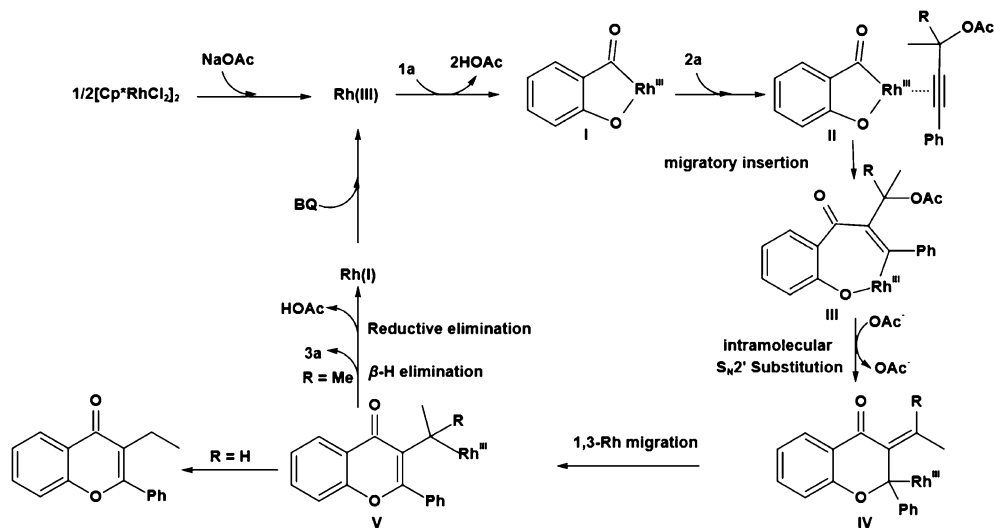


Figure 1. Calculated free energy profiles of possible pathways starting catalyst (cat) and substrate (1a), in which the red path is calculated for O₂-coordination and the black path is for O₁-coordination for C–H deprotonation and C–H activation. Key bond lengths (Å) and insignificant H atoms have been omitted for clarity purposes. Additional geometries not included in the text can be found in Figure S2.

this study, our primary focus lies on the following inquiries: (1) regioselectivity regarding propargylic acetate insertion to the Rh–C bond, (2) elucidating the role played by acetate in

intramolecular S_N2' cyclization from intermediate III to IV, (3) identifying rate- and selectivity-determining steps, (4) comprehending how methyl as an assisting group influences β-

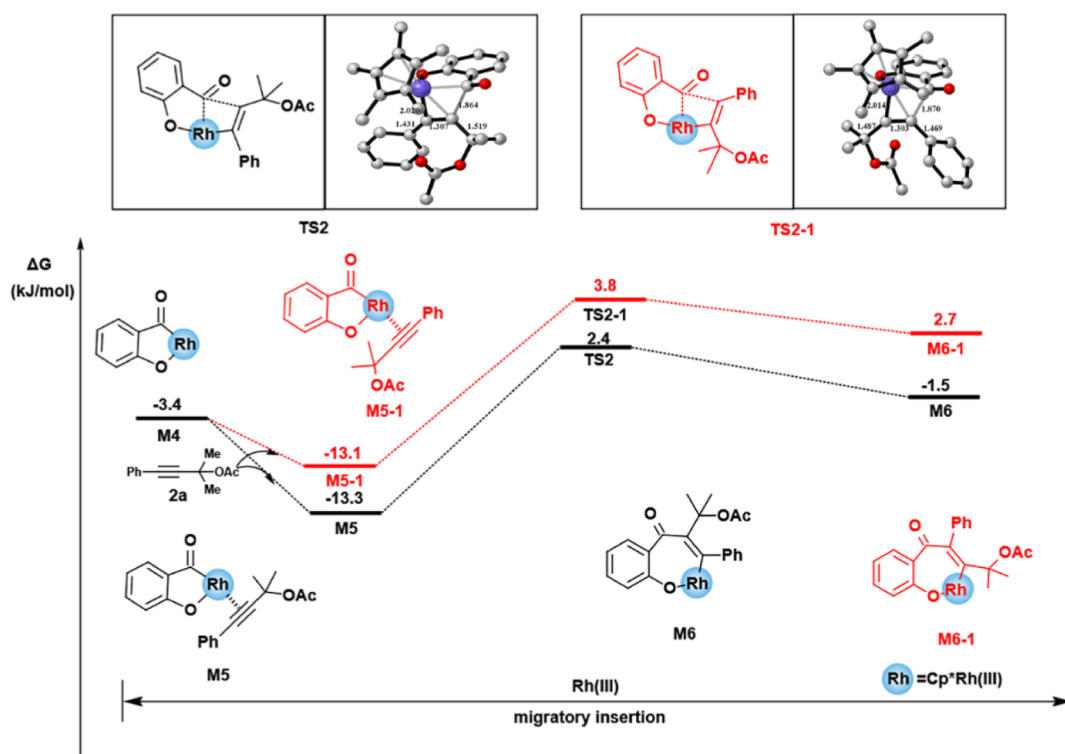


Figure 2. Free energy profile for the insertion of an alkyne into the Rh–C bond is presented, with relative free energies reported in kcal/mol. Key bond lengths (Å) and insignificant H atoms have been omitted for clarity purposes. Additional geometries not included in the main text can be found in Figure S3.

H elimination in intermediate V, and (5) exploring how substituent at the C_{α} position impacts product yield.

COMPUTATIONAL DETAILS

The DFT calculations were conducted using the Gaussian 16 software package,¹³ with geometry optimizations performed in the gas phase employing the B3LYP^{14,15} and D3(BJ) dispersion correction.^{16,17} The Rh atom was described by the LanL2DZ basis set,^{18,19} while nonmetal atoms utilized the 6-31G(d) basis set. Polarization functions²⁰ were included for Rh ($\zeta_f = 1.350$). Harmonic vibrational frequencies were calculated at the same level as geometry optimizations to characterize each stationary point as a minimum and to obtain the thermodynamic corrections to Gibbs free energy. For more accurate relative energies, single-point energies were computed using the M06^{21–23} functional combined with a larger basis set (SDD^{24,25} basis set for Rh and 6-311++G(d,p) for the remaining atom), while considering the solvation effect of dichloromethane (DCM) through the SMD²⁶ solvation model. The reported Gibbs free energy in solution incorporates gas-phase free-energy corrections. The three-dimensional molecular structures presented in this study were generated using CYLview.²⁷

RESULTS AND DISCUSSION

We conducted a comprehensive mechanistic study on the target reaction (Scheme 1) using salicylaldehyde **1a** and propargylic acetate **2a** (**2a-H**) as the model substrates while employing the CpRh*(III) catalyst to facilitate catalytic effects.

Starting from the catalytically active species CpRh(OAc)₂ (**cat**), which is generated through [CpRhCl₂]₂, it reacts with NaOAc through chloride abstraction by Na⁺ and ligand

exchange. The catalytically active substance **cat** first interacts with **1a** to form the O1-coordination intermediate **M1** or the O2-coordination isomer **M1–1** (Figure 1 and Figure S1, see Supporting Information for Figure 1). According to Figure 1, computational results indicate that the relative energies of **M1** and **M1–1** are -1.7 and 5.5 kcal/mol, respectively, indicating that intermediate **M1** coordinated with O1 is more stable. Meanwhile, a natural population analysis (NPA) population analysis was also performed on the salicylaldehyde substrate (Figure 2). The charges of the O1 atom and the O2 atom were determined to be -0.675 and -0.529 e, respectively. It can be observed that the electronegativity of the O1 atom is stronger, making it easier for the O1 atom to coordinate with the Rh center. Therefore, we consider only the most stable isomer, **M1**. The catalyst coordination is followed by deprotonation of the O–H and dissociation of acetic acid (HOAc) from the **M1**. During the coordination process, acetic acid snatches an H atom from the hydroxyl group, thus shedding an HOAc to form the intermediate **M2**. Subsequently, concerted metalation-deprotonation (CMD) occurs via **TS1** ($\Delta G^{\ddagger} = 14.8$ kcal/mol), leading to the cleavage of the C–H bond and the formation of **M3** at -7.8 kcal/mol relative to **M1**. Acetic acid dissociation gives rise to the five-membered rhodacycle **M4**.

The regioselectivity for migration insertion of asymmetric propargylic acetates (**2a**) into the Rh–C bond was also taken into consideration, as depicted in Figure 2. In the alkynyl insertion process, coordination may result in the formation of alkynyl-coordinated π -complexes **M5** or **M5–1**. Then, insertion of **2a** into the Rh–C bond occurs via both 2,1-insertion (resulting in C3-functionalized chromones) and 1,2-insertion (resulting in C4-functionalized chromones, shown in red). The energy profile clearly demonstrates that the 2,1-insertion pathway through **TS2** ($\Delta G^{\ddagger} = 15.7$ kcal/mol) is

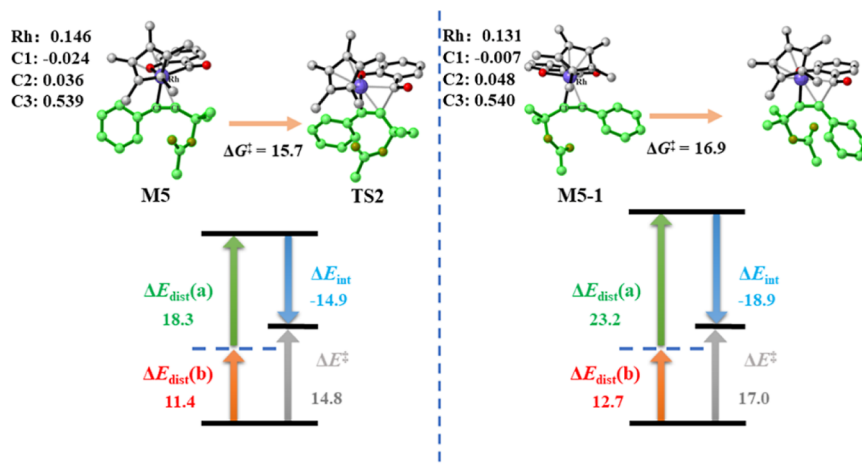


Figure 3. Distortion–interaction analysis was performed for the transition states of TS2 and TS2–1, with the energies reported in kcal/mol. Additionally, the NPA charge (e) was determined for the optimized structures of M5 and M5–1. The H atoms were excluded from the 3D structures to enhance clarity.

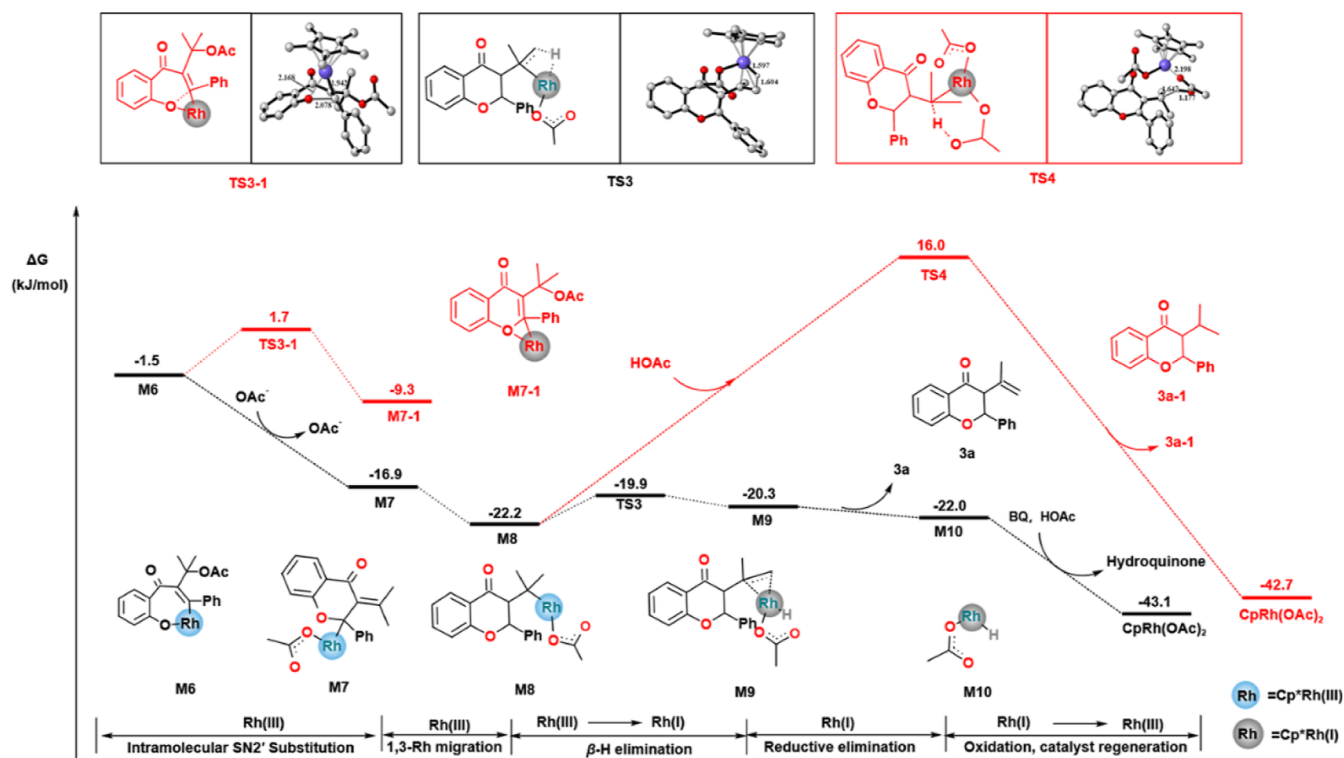


Figure 4. Free energy profile for the intramolecular $\text{S}_{\text{N}}2'$ substitution, 1,3-Rh migration, β -H elimination, and reductive elimination processes is presented. The relative free energies are reported in kcal/mol. Key bond lengths (Å) and trivial H atoms have been omitted for clarity. Additional geometries not shown in the main text can be found in Figure S3.

more favorable than the 1,2-insertion pathway through TS2–1 ($\Delta G^\ddagger = 16.9$ kcal/mol), with a difference of 1.2 kcal/mol. Furthermore, the alkyne insertion step determines regioselectivity. These findings are consistent with the experimental observations where the Cp*Rh(III) catalyst was used to obtain the C3-functionalized chromones. The preferred alkynyl's 2,1-insertion leads to the formation of a seven-membered rhodacycle M6. The alternative pathway of alkyne insertion into the Rh–O bond is not viable (Figure S4).

We also investigated the origin of regional effects in the Cp*Rh(III)-catalytic systems. The distortion–interaction analysis²⁸ was additionally conducted on the intermediate

and transition state structures of the alkyne insertion pathways of M5, M5–1, TS2, and TS2–1. These structures were divided into two fragments: the propargylic acetate portion (fragment a, highlighted in green in Figure 3), and the remaining catalytic cationic Rh(III) moiety (fragment b). ΔE_{int} represents the difference in the interaction energies between the two components in M5 (M5–1) and TS2 (TS2–1), and ΔE_{dist} denotes the energy required to distort the fragment (a or b) from M5 (M5–1) to TS2 (TS2–1). The corresponding structures and energy analysis results are listed in Figure 3. In transition state TS2, the interaction energy (ΔE_{int}) is –14.9 kcal/mol, with a distortion energy of fragment a ($\Delta E_{\text{def}}(\text{a})$) at

11.4 kcal/mol, a distortion energy of fragment **b** ($\Delta E_{\text{def}(\text{b})}$) at 18.3 kcal/mol, and a total distortion energy for both fragments ($\Delta E_{\text{def}(\text{a+b})}$) at 29.7 kcal/mol. The activation energy ΔE^\ddagger is defined as $\Delta E^\ddagger = \Delta E_{\text{dist}(\text{a})} + \Delta E_{\text{dist}(\text{b})} + \Delta E_{\text{int}} = 14.8$ kcal/mol. The results indicate that the interaction between the two fragments in **TS2-1** (18.9 kcal/mol) is greater than that in **TS2** (14.9 kcal/mol), with a difference of 4.0 kcal/mol observed. Furthermore, the distortion energies of fragments **a** and **b** in **TS2-1** are higher by 4.9 and 1.3 kcal/mol, respectively, compared to those in **TS2**, highlighting their significant contribution to the disparity in energy barriers between **TS2** and **TS2-1**. The ΔE^\ddagger values of the two transition states, as depicted in Figure 3, align with the observed trends in their respective free energy barriers (ΔG^\ddagger). Additionally, Figure 3 presents the NPA charges of **M5** and **M5-1** on the atoms involved in Rh–C3 and C1≡C2 bonds that participate in alkynyl migratory insertion. It is evident that attractive interactions inferred from the NPA charge distribution of C1 δ^- –C3 δ^+ in **M5** facilitate alkynyl insertion, whereas C2 δ^+ –C3 δ^+ in **M5-1** does not promote such insertion. Further results demonstrate that both the CMD step and the alkynyl insertion steps exhibit the two highest barriers among the whole reaction.

The calculations were subsequently conducted to further scrutinize the mechanistic aspects of current oxidative C–O bond formation. The reaction mechanisms of the two pathways are illustrated in Figure 4. It was determined that a barrier energy of 3.1 kcal/mol is required for the direct process from **M6**. The bond orders of the Rh–C and Rh–O bonds in Cp*Rh(III) intermediate **M6** are found to be 1.079 and 0.759, respectively, indicating that their strengths are determined. Moreover, NPA charge distribution analysis reveals that the presence of C δ^+ –O δ^+ in **M6** is unfavorable for C–O bond formation. However, with assistance from OAc $^-$, which strongly coordinates with the Rh center, it undergoes an S_N2' intramolecular cyclization to form a stable six-membered intermediate **M7** with an exoergic energy release of 15.4 kcal/mol facilitated by just OAc $^-$. Next, **M7** undergoes 1,3-Rh migration to produce a more stable intermediate **M8**. The formation of **M8** exhibits a significant exoergic effect, with an energy release of 22.2 kcal/mol, thereby providing a thermodynamic driving force for promoting the progression of the reaction.

Subsequently, β -H elimination occurs via **TS3** to yield the intermediate complex **M9**, featuring a newly formed olefin bond with a ΔG^\ddagger value of 2.2 kcal/mol. Simultaneously, the Rh center undergoes reduction by two electrons, resulting in an oxidation state of +1. Finally, the dissociation of the **3a** product from complex **M9** and the formation of Cp*Rh(I) complex **M10** take place through a thermodynamically favorable process with a ΔG of –1.7 kcal/mol. It is widely accepted that under the BQ and HOAc conditions, Cp*Rh(I) complex **M10** can be oxidized by two electrons to regenerated Cp*Rh(OAc)₂ and participate in the subsequent catalytic cycle. Additionally, Figure 4 illustrates that in complex **M9**, the HOAc molecular coordinates with the Rh center through transition state **TS4**, leading to the dissociation of Cp*Rh(OAc)₂ and the formation of **3a-1** (highlighted in red). The findings indicate that the process of generating product **3a-1** is dynamically unfavorable due to an insurmountably high calculated barrier ($\Delta G^\ddagger = 38.2$ kcal/mol). However, in the case of R = H (Scheme 2, Figure S6 in the Supporting Information), the coordination of HOAc to the Rh center via

transition state **TS3-1-H** to form **14** is kinetically feasible with a barrier of 23.2 kcal/mol, and the total free energy value of **TS3-1-H** is –4.9 kcal/mol. Therefore, when R = H, besides yielding product **13**, it is crucial not to overlook the formation of byproduct **14**. This implies that substituents on the C_α can effectively impede the generation of byproducts due to steric hindrance effects.

CONCLUSIONS

The reaction mechanism of the Cp*Rh(III)-catalyzed C–H functionalization of salicylaldehydes with propargylic acetate to form 3-vinyl chromones has been theoretically investigated by using DFT calculations. The study revealed that the reaction proceeds through the following steps: C–H activation via CMD, 2,1-alkyne migratory insertion, intramolecular S_N2' substitution, 1,3-Rh migration, β -H elimination, reductive elimination, and catalyst regeneration for the next catalytic cycle. The highest barrier throughout the entire catalysis process is estimated to be 13.4 kcal/mol (cat + **1a** → **M1** → **M2** → **TS1**), indicating that the CMD step is the rate-determining step (RDS) for this reaction. This in-depth mechanistic study will facilitate further exploration of their reactivity in the presence of other coupling partners in the search for novel cascade transformations to expand the chemical space of O-heterocycles.

ASSOCIATED CONTENT

Data Availability Statement

The data supporting this study can be found in the published article and its accompanying Supporting Information.

Supporting Information

The Supporting Information is available free of charge at <https://pubs.acs.org/doi/10.1021/acsomega.3c07381>.

NPA, Cartesian coordinates of all stationary points, and their corresponding single-point energies (a.u.) in solution (PDF)

AUTHOR INFORMATION

Corresponding Author

Zeng-Xia Zhao – Laboratory of Theoretical and Computational Chemistry, Institute of Theoretical Chemistry, College of Chemistry, Jilin University, Changchun 130023, P. R. China; orcid.org/0000-0003-1276-828X; Phone: +86-0431-88498962; Email: zhaozx@jlu.edu.cn

Authors

Xin Xiang – Laboratory of Theoretical and Computational Chemistry, Institute of Theoretical Chemistry, College of Chemistry, Jilin University, Changchun 130023, P. R. China

Wei Wei – Laboratory of Theoretical and Computational Chemistry, Institute of Theoretical Chemistry, College of Chemistry, Jilin University, Changchun 130023, P. R. China; orcid.org/0000-0002-1387-7077

Hong-Xing Zhang – Laboratory of Theoretical and Computational Chemistry, Institute of Theoretical Chemistry, College of Chemistry, Jilin University, Changchun 130023, P. R. China; orcid.org/0000-0001-5334-733X

Complete contact information is available at:

<https://pubs.acs.org/doi/10.1021/acsomega.3c07381>

Notes

The authors declare no competing financial interest.

ACKNOWLEDGMENTS

We are extremely grateful to the Institute of Theoretical Chemistry, College of Chemistry, Jilin University, for providing us with computational resources.

REFERENCES

- (1) Gaspar, A.; Matos, M. J.; Garrido, J.; Uriarte, E.; Borges, F. Chromone: A Valid Scaffold in Medicinal Chemistry. *Chem. Rev.* **2014**, *114* (9), 4960–4992.
- (2) Reis, J.; Gaspar, A.; Milhazes, N.; Borges, F. Chromone as a Privileged Scaffold in Drug Discovery: Recent Advances. *J. Med. Chem.* **2017**, *60* (19), 7941–7957.
- (3) Li, X.; Shen, Y.; Zhang, G.; Zheng, X.; Zhao, Q.; Song, Z. Ru(II)-Catalyzed Decarbonylative Alkylation and Annulations of Benzaldehydes with Iodonium Ylides under Chelation Assistance. *Org. Lett.* **2022**, *24* (29), 5281–5286.
- (4) Pali, P.; Yadav, D.; Sahoo, S. C.; Shankar Singh, M. Metal-Free One-Pot Annulative Coupling of 2-Hydroxybenzaldehydes with β -Ketothioamides: Access to Diverse 2-Arylimino-2H-Chromenes. *J. Org. Chem.* **2022**, *87* (18), 12342–12351.
- (5) Chang, Z.-X.; Li, F.-R.; Xia, C.; Li, F.; Li, H.-S. Regioselective Access to 3-Ethylidene-flavanones via Rhodium(I)-Catalyzed 1,3-Enyne Hydroacylation/Annulation Cascades. *Adv. Synth. Catal.* **2021**, *363* (6), 1722–1726.
- (6) Meng, J.; Ding, X.; Yu, X.; Deng, W.-P. Synthesis of 2,5-epoxy-1,4-benzoxazepines via rhodium(II)-catalyzed reaction of 1-tosyl-1,2,3-triazoles and salicylaldehydes. *Tetrahedron* **2016**, *72* (1), 176–183.
- (7) Zhao, S.; Cai, X.; Lu, Y.; Hu, J.; Xiong, Z.; Jin, J.; Li, Y.; Wang, H.; Wu, J.-Q. Cp*Ir(III) and Cp*Rh(III)-catalyzed annulation of salicylaldehydes with fluorinated vinyl tosylates. *Chem. Commun.* **2022**, *58* (64), 8966–8969.
- (8) Sosnovskikh, V. Y. Synthesis and Reactivity of Electron-Deficient 3-Vinylchromones. *SynOpen* **2021**, *05* (03), 255–277.
- (9) Yu, Y.-F.; Zhang, C.; Huang, Y.-Y.; Zhang, S.; Zhou, Q.; Li, X.; Lai, Z.; Li, Z.; Gao, Y.; Wu, Y.; Guo, L.; Wu, D.; Luo, H.-B. Discovery and Optimization of Chromone Derivatives as Novel Selective Phosphodiesterase 10 Inhibitors. *ACS Chem. Neurosci.* **2020**, *11* (7), 1058–1071.
- (10) Kumar, S.; Verma, N.; Zubair, S.; Faisal, S. M.; Kazmi, S.; Chakraborty, S.; Owais, M.; Ahmed, N. Design and Synthesis of Novel Nonsteroidal Phytoestrogen-based Probes as Potential Biomarker: Evaluation of Anticancer Activity and Docking Studies. *J. Heterocycl. Chem.* **2017**, *54* (4), 2242–2257.
- (11) Talhi, O.; Brodziak-Jarosz, L.; Panning, J.; Orlikova, B.; Zwergel, C.; Tzanova, T.; Philippot, S.; Pinto, D. C. G. A.; Paz, F. A. A.; Gerhäuser, C.; Dick, T. P.; Jacob, C.; Diederich, M.; Bagrel, D.; Kirsch, G.; Silva, A. M. S. One-Pot Synthesis of Benzopyran-4-ones with Cancer Preventive and Therapeutic Potential. *Eur. J. Org. Chem.* **2016**, *2016* (5), 965–975.
- (12) Li, B.; Zhu, J.; Zheng, X.; Ti, W.; Huang, Y.; Yao, H. Rh(III)-Catalyzed Oxidative C-H Activation/Annulation of Salicylaldehydes with Masked Enynes for the Synthesis of Chromones. *J. Org. Chem.* **2023**, *88* (1), 548–558.
- (13) Frisch, M. J.; Trucks, G. W.; Schlegel, H. B.; Scuseria, G. E.; Robb, M. A.; Cheeseman, J. R.; Scalmani, G.; Barone, V.; Petersson, G. A.; Nakatsuji, H.; Li, X.; Caricato, M.; Marenich, A. V.; Bloino, J.; Janesko, B. G.; Gomperts, R.; Mennucci, B.; Hratchian, H. P.; Ortiz, J. V.; Izmaylov, A. F.; Sonnenberg, J. L.; Williams, D. J.; Ding, F.; Lipparini, F.; Egidi, F.; Goings, J.; Peng, B.; Petrone, A.; Henderson, T.; Ranasinghe, D.; Zakrzewski, V. G.; Gao, J.; Rega, N.; Zheng, G.; Liang, W.; Hada, M.; Ehara, M.; Toyota, K.; Fukuda, R.; Hasegawa, J.; Ishida, M.; Nakajima, T.; Honda, Y.; Kitao, O.; Nakai, H.; Vreven, T.; Throssell, K.; Montgomery, Jr., J. A.; Peralta, J. E.; Ogliaro, F.; Bearpark, M. J.; Heyd, J. J.; Brothers, E. N.; Kudin, K. N.; Staroverov, V. N.; Keith, T. A.; Kobayashi, R.; Normand, J.; Raghavachari, K.; Rendell, A. P.; Burant, J. C.; Iyengar, S. S.; Tomasi, J.; Cossi, M.; Millam, J. M.; Klene, M.; Adamo, C.; Cammi, R.; Ochterski, J. W.; Martin, R. L.; Morokuma, K.; Farkas, O.; Foresman, J. B.; Fox, D. J. *Gaussian 16 Rev. A.03*: Wallingford, CT, 2016.
- (14) Becke, A. D. Density-functional thermochemistry. III. The role of exact exchange. *J. Chem. Phys.* **1993**, *98* (7), 5648–5652.
- (15) Lee, C.; Yang, W.; Parr, R. G. Development of the Colle-Salvetti correlation-energy formula into a functional of the electron density. *Phys. Rev. B* **1988**, *37* (2), 785–789.
- (16) Grimme, S.; Ehrlich, S.; Goerigk, L. Effect of the damping function in dispersion corrected density functional theory. *J. Comput. Chem.* **2011**, *32* (7), 1456–1465.
- (17) Grimme, S.; Antony, J.; Ehrlich, S.; Krieg, H. A consistent and accurate ab initio parametrization of density functional dispersion correction (DFT-D) for the 94 elements H-Pu. *J. Chem. Phys.* **2010**, *132* (15), 154104.
- (18) Wadt, W. R.; Hay, P. J. Ab initio effective core potentials for molecular calculations. Potentials for main group elements Na to Bi. *J. Chem. Phys.* **1985**, *82* (1), 284–298.
- (19) Hay, P. J.; Wadt, W. R. Ab initio effective core potentials for molecular calculations. Potentials for K to Au including the outermost core orbitals. *J. Chem. Phys.* **1985**, *82* (1), 299–310.
- (20) Ehlers, A. W.; Böhme, M.; Dapprich, S.; Gobbi, A.; Höllwarth, A.; Jonas, V.; Köhler, K.; Stegmann, R.; Veldkamp, A.; Frenking, G. A set of f-polarization functions for pseudo-potential basis sets of the transition metals Sc—Cu, Y—Ag and La—Au. *Chem. Phys. Lett.* **1993**, *208* (1–2), 111–114.
- (21) Zhao, Y. J.; Zhang, Z. M.; Ding, Z. J.; Zhang, Q. Raman scattering study of colloidal MoS₂ under high pressure. *Chin. J. High Pressure Phys.* **2007**, *21* (2), 215–219.
- (22) Zhao, Y.; Truhlar, D. G. Benchmark Energetic Data in a Model System for Grubbs II Metathesis Catalysis and Their Use for the Development, Assessment, and Validation of Electronic Structure Methods. *J. Chem. Theory Comput.* **2009**, *5* (2), 324–333.
- (23) Zhao, Y.; Truhlar, D. G. Density Functionals with Broad Applicability in Chemistry. *Acc. Chem. Res.* **2008**, *41* (2), 157–167.
- (24) Dolg, M.; Wedig, U.; Stoll, H.; Preuss, H. Energy-adjusted ab initio pseudopotentials for the first row transition elements. *J. Chem. Phys.* **1987**, *86* (2), 866–872.
- (25) Andrae, D.; Häußermann, U.; Dolg, M.; Stoll, H.; Preuß, H. Energy-adjusted ab initio pseudopotentials for the second and third row transition elements. *Theor. Chim. Acta* **1990**, *77* (2), 123–141.
- (26) Marenich, A. V.; Cramer, C. J.; Truhlar, D. G. Universal Solvation Model Based on Solute Electron Density and on a Continuum Model of the Solvent Defined by the Bulk Dielectric Constant and Atomic Surface Tensions. *J. Phys. Chem. B* **2009**, *113* (18), 6378–6396.
- (27) Legault, C. Y. CYLview20. <http://www.cylview.org> (accessed 2020).
- (28) Bickelhaupt, F. M.; Houk, K. N. Analyzing Reaction Rates with the Distortion/Interaction-Activation Strain Model. *Angew. Chem., Int. Ed.* **2017**, *56* (34), 10070–10086.